Enhanced photocatalytic performance of novel electrospun BN/TiO 2 composite nanofibers

Maryline Nasr, Roman Viter, Cynthia Eid, Roland Habchi, Philippe Miele, Mikhael Bechelany

Enhanced photocatalytic performance of novel electrospun BN/TiO_2 composite nanofibers

Received 00th January 20xx,
Accepted 00th January 20xx

DOI : 10.1039/x0xx00000x

www.rsc.org/

Maryline Nasr,[†a,b] Roman Viter,[c] Cynthia Eid,[b] Roland Habchi,[b] Philippe Miele,[a] Mikhael Bechelany[†a]

High activity Boron nitride**/**Titanium dioxide (BN/TiO_2) composite nanofibers photocatalysts were successfully synthesized for the first time via the electrospinning technique. The as-spun nanofibers with controlled ratio of boron nitride nanosheets (BN) were calcined under air at 500°C for 4 hours. Their morphological, structural and optical properties were studied by Scanning electron microscopy (SEM), X-ray diffraction (XRD), Energy-dispersive X-ray spectroscopy (EDX), BET surface area, Fourier-transform infrared (FTIR), Raman spectroscopy, UV-Visible spectrophotometer and Room temperature photoluminescence (PL). The effect of loading different BN sheets amounts on the photocatalytic degradation of methyl orange (MO) was investigated. The results indicated that the presence of BN sheets improves the separation of the photo-induced electron–hole pairs in TiO_2 and increases the band gap energy and the specific surface area compared to the pure TiO_2 nanofibers. BN/TiO_2 (wt. 10%) composite nanofibers photocatalytic activity is enhanced to 99% compared to 60% and 65% for P25 and TiO_2 nanofibers, respectively. Thus, the composites BN/TiO_2 significantly increases the UV light photo-response and improves the separation of photo-induced electron-hole pairs of TiO_2.

Introduction

The availability of safe drinking water is a high priority issue for human existence and quality of life. Until now, water pollution becomes more and more serious with the emission of large amount of organic pollutants due to the rapid development of agriculture and industry. Therefore, it is desirable to develop an effective method to deal with organic pollutions. In this context, photocatalysis is gradually developed as a new environmental protection technology since the 1970's because it can play an important role in solar energy conversion and degradation of organic pollutants[1]. Titanium oxide (TiO_2) has drawn the maximum attention as photocatalyst, due to its relatively low cost, high stability and low toxicity[2]. TiO_2 has been widely used in many applications including dye-sensitized solar cells, gas sensors, biofuel cells, biomaterials and most notably as a photocatalyst in UV spectrum.[3-6] However, the fast electron–hole pair recombination of TiO_2 significantly limits the efficiency of the photocatalytic reaction[7]. This limitation have been often overcome by doping TiO_2 with nobel metals or other semiconductor materials such as Ag[8], Pt[9], NiO[10], SnO_2[11] and graphene[12]. This is one of the most effective methods to increase the separation efficiency of photogenerated electron-hole pairs in order to enhance the photocatalytic activities of TiO_2.

Researchers have recently devoted attention to 2D Boron nitride nanosheets, which have structural similarities to graphene. The white graphene (monolayer of BN) is an individual BN basal plane in which C atoms have been replaced by alternating B and N atoms[13,14]. Many extraordinary properties can arise from the BN nanosheets due to the high surface area and the reactive edge structure[15]. BN nanosheets demonstrate high temperature, high chemical stability, high onset temperature of oxidation (> 850 °C), high electrical resistance and wide band gap (> 5.5 eV)[16,17]. These properties make BN nanosheets very appealing in wide range of applications such as nanoelectronic, optoelectronic devices and nanocomposites[15]. Recently, Fu et *al*.[18] prepared the h-BN/TiO_2 composite photocatalyst by ball milling method[19]. They reported that due to the electrostatic interaction, the charged h-BN can promote the migration of h^+ from TiO_2 bulk to its surface and consequently improve the photocatalytic activity. Tang et *al*.[20] synthesized nanocrystalline TiO_2 attached to BN nanotubes using hydrolysis of $TiCl_3$ aqueous solution at 80°C in the presence of esterified BN nanotubes.

Various TiO_2 nanostructures (0D, 1D, 2D and 3D) have been synthesized such as nanotubes[21], hollow hemispheres[22], nanorods[23] and nanofibers.[24] Several techniques have been developed for the fabrication of these TiO_2 nanostructures, such as hydrothermal method, vapor-thermal treatment, colloidal templating method, solvothermal method and electrospinning.[22-28] Thian et *al*.[29] synthesized for instance 3D hierarchical flower-like TiO_2 nanostructures via a facile solvothermal method combining a calcination process. Reddy *et al*.[30,31] used an electrospinning technique for fabricating 1D TiO_2 nanofibers for photocatalytic application. Among all these techniques, electrospinning is a simple and cost-effective technique. It permits the synthesis of nanofibers with controllable diameter ranging from a few to several hundred of nanometers, depending on the polymer and processing conditions[32].

In the present work, we report on a novel photocatalytic composite nanofibers BN nanosheets/TiO_2 prepared via electrospinning. However, to our knowledge, there is no study concerning the preparation of BN nanosheets/TiO_2 composite nanofibers. Exfoliated boron nitride sheets were obtained by

[a.] *Institut Européen des Membranes IEM UMR-5635, Université de Montpellier, ENSCM, CNRS, Place Eugène Bataillon, F-34095 Montpellier Cedex 5, France.*
[b.] *EC2M, faculty of sciences 2, and Research Platform for Nanosciences and Nanotechnologies, campus Pierre Gemayel, Fanar, Lebanese University, 90656 Lebanon.*
[c.] *Institute of Atomic Physics and Spectroscopy, University of Latvia, 19 Raina Blvd., LV 1586 Riga, Latvia*
† Corresponding authors: Maryline Nasr, maryline.nasr@hotmail.com at the Lebanese University and Mikhael Bechelany, mikhael.bechelany@univ-montp2.fr at the university of Montpellier.

our original method based on high power ultrasonication of boron nitride nanopowder with gelatine[15,13]. The BN/TiO_2 composite nanofibers with different amounts of boron nitride (0, 3, 5, 7 and 10 wt. % of the mass of Ti) have been elaborated by using electrospinning technique. All the samples were annealed at 500°C in air for 4 hours. The structural, morphological and optical properties of the prepared samples were analysed. The performances of these materials for photocatalytic degradation of methyl orange under UV light have also been evaluated.

Experimental

Chemicals and Materials

Commercial boron nitride (95%, 325 mesh), titanium tetraisopropoxide (TTIP) $Ti\{OCH(CH_3)_2\}_4$ (97%), polyvinylpyrrolidone (PVP) (Mw = 13,00,000), acetic acid (98%), Gelatine from porcine skin, methyl orange and absolute ethanol were purchased from Sigma Aldrich, and used without any further purification.

Exfoliation of Boron nitride

Boron nitride sheets were exfoliated from boron nitride powder[15,13]. Briefly, 20g of gelatine were dissolved in 80 ml of hot water (75°C). After gelatine dissolving, 1g of boron nitride powder was added to the mixture. The solution was kept in an ultrasonic homogenizer over night at 50°C. Exfoliated BN was separated by centrifugation at 2697 G for 30 minutes and the supernatant was decanted away. The resultant precipitates were dried at 80°C for 48 hours and then calcined at 600°C in air for 2 hours in order to obtain the pure exfoliated boron nitride.

Preparation of TiO_2 and BN composite nanofibers

The BN-incorporated TiO_2 nanofibers were synthesized by an electrospinning technique. The spun solution was prepared as follows: different amounts of boron nitride (0, 3, 5, 7 and 10 wt. % of the mass of Ti) and 2 ml of absolute ethanol were homogenized for 12h to disperse boron nitride into the ethanol solution. Titanium tetraisopropoxide was dissolved in a mixture of 2 ml of acetic acid and 3 ml of ethanol mixed with 0.3 g of polyvinylpyrrolidone (PVP). The precursor mixture was stirred for 1 h at room temperature to obtain sufficient viscosity required for electrospinning. Finally, the BN solution was added to the precursor solution under vigorous magnetic stirring (150 rpm) for 30 min. The homogeneous solution was typically extruded through a stainless steel nozzle with a diameter of 0.7 mm at a constant flow rate of 1 ml/h. The feeding rate was controlled by the syringe pump. The temperature level inside the electrospinning chamber was 38 ± 5°C. Nanofibers were collected on a rotating coil covered with an aluminium foil with a rotation speed of 400 rpm. The distance between the tip of the needle and the aluminium foil was maintained at 20 cm, and a DC voltage of 25 kV was applied. In the electrospinning process, the high applied voltage was achieved by connecting the positive and ground terminals to the nozzle and collector, respectively. During electrospinning, the applied electric field overcomes the surface tension of the polymeric solution, thereby ejecting a continuous jet which upon subsequent solvent evaporation and bending produces nanofibers on the collector surface. The electrospun BN-TiO_2 composite nanofibers were collected and then calcined in a tubular furnace at 500°C with a heating rate of 5°C/min for 5 h in air.

Physical and Chemical Characterization

X-ray diffraction (XRD) measurements were carried out using a PANAlytical Xpert-PRO diffractometer equipped with an X'celerator detector using Ni-filtered Cu-radiation (λ= 1.54 ˚A). Fourier-transform infrared (FTIR) spectra were recorded on a Nicolet 370 FTIR spectrometer using an ATR system. Raman spectra have been obtained from Horiba, λ= 659 nm. Scanning electron microscopy (SEM) images were taken with a Hitachi S4800, Japan. Energy-dispersive X-ray spectroscopy analysis (EDX) and elemental mapping were taken with Zeiss EVO HD15 microscope coupled with an Oxford X-MaxN EDX detector. The UV–VIS absorbance spectra were recorded by a Jasco V-570 UV–VIS-NIR spectrophotometer. The surface area of samples was determined from nitrogen adsorption-desorption isotherms at liquid nitrogen temperature using micromeritrics ASAP 2010 equipment (outgassing conditions: 200°C-12h). Room temperature photoluminescence (PL) has been measured in the range of 370-800 nm. The PL was excited with nitrogen Nd:YAG laser (266 nm, 10 mW, 1 kHz) and recorded with optical fiber spectrometer (Ocean Optics usb2000).

Photocatalytic activity measurement

Methyl orange (MO) was used as a reference of organic pollutant to evaluate the photocatalytic activity of the BN/TiO_2 composite nanofibers. The photocatalytic performance of the samples was evaluated by analyzing the decrease in concentration of the MO during exposure to UV light irradiation. The reaction temperature was kept constant at 25 ± 0.2 °C by circulating water in a cylindrical tube surrounding the photo-reactor during the entire experiment. The decomposition was carried out in several beakers containing a suspension of 10 mg of each sample in 25 ml of MO solution (10 mg/L) under visible light irradiation (obtained from a 48 W light source, emission wavelength < 400 nm). The distance between the lamp and the dye solution was maintained at 10 cm. First, the solution mixture was magnetically stirred for 30 min without irradiation to reach the adsorption–desorption equilibrium of MO. Then the solution was irradiated with visible light for 75 minutes. Each 15 min, 3 ml of the sample solution was taken out and centrifuged to remove the catalyst. The centrifuged solutions were analyzed by a UV-VIS spectrometer. The absorbance spectra of MO (major absorption band around 462 nm)[33] were recorded to measure the change in the concentration of MO[34]. After irradiation, the photocatalytic degradation efficiency has been calculated as follows:

Degradation efficiency (%) = $(C_0 - C) / C_0 \times 100$ (Equation 1)

where C_0 and C are the initial concentration and the final concentration of dye before and after photo-irradiation

respectively[35]. This equation shows the dye photocatalyst degradation percentage.

Results and discussion

The TiO_2 and BN/TiO_2 NFs with different amounts of boron nitride were obtained by electrospinning of a solution of polymer with titanium tetraisopropoxide as precursor. Scanning electron microscopy was used to investigate the morphological features of TiO_2 and BN/TiO_2 nanofibers. Figure 1 shows the SEM images of the obtained TiO_2 and BN-containing electrospun nanofibers after calcinations in air at 500°C for 4 hours. The formation of highly interconnected networks of continuous, randomly oriented nanofibers can be clearly seen. As illustrated in Figure 1, the nanofibrous morphology was largely preserved after the heat treatment process. The fiber diameters were measured from the SEM images using image analysis software (Image J1.29X). The average diameter was measured on 100 randomly chosen nanofibers of each sample (Figure 1). After calcination, we measure average diameters of (187 ± 5 nm), (229 ± 7nm), (269 ± 10 nm), (290 ± 13 nm) and (314 ± 15 nm) for samples with BN weight amount of 0, 3, 5, 7 and 10 wt. %, respectively. In fact, the average diameter of the nanofibers increases with the increase of boron nitride amount. This can be attributed to the increase of the solution viscosity induced by inclusion of BN in the electrospinning solution[2]. This increase reveals the successful incorporation of BN in TiO_2 nanofibers.

Table 1. EDX data showing the composition of TiO_2, BN (3 wt. %)/TiO_2, BN (5wt. %)/TiO_2, BN (7wt. %)/TiO_2 and BN (10 wt. %)/TiO_2 annealed nanofibers under air

	Atomic percentages				
Samples	Ti	O	C	B	N
TiO_2	33.42	61.28	5.3	_	_
BN (3 wt. %)	26.59	53.67	4.16	8.4	7.18
BN (5 wt. %)	24.81	52.45	6.31	9.23	7.2
BN (7 wt. %)	23.84	48.25	5.48	10.59	11.84
BN (10 wt. %)	25.0 5	46.19	5.13	12.14	11.49

An energy dispersive X-ray spectrum (EDX) of BN/TiO_2 nanofibers recorded along with elemental analysis is presented in Table 1. The EDX analysis reveals the molar ratio of Ti and O to be 1:2 for the above described fibers, which is in good agreement with the stoichiometric ratio of TiO_2. Also, the BN doped fibers have a molar ratio of 1:1 for boron and nitrogen. The increase of the atomic percentages of B and N in BN (3 wt. %) /TiO_2, BN (5wt. %)/TiO_2, BN (7wt. %)/TiO_2 and BN (7wt. %)/TiO_2 can be clearly seen from table 1. Figure 2 shows elemental mapping images on BN (5wt. %)/TiO_2 Nanofibers. These images clearly shows that Ti, O, B and N elements evenly spread over the entire area of the sample confirming the good dispersion of BN nanosheets in the TiO_2 Nanofibers. Based on these data, the BN/TiO2 composite nanofibers were successfully fabricated using the electrospinning method.

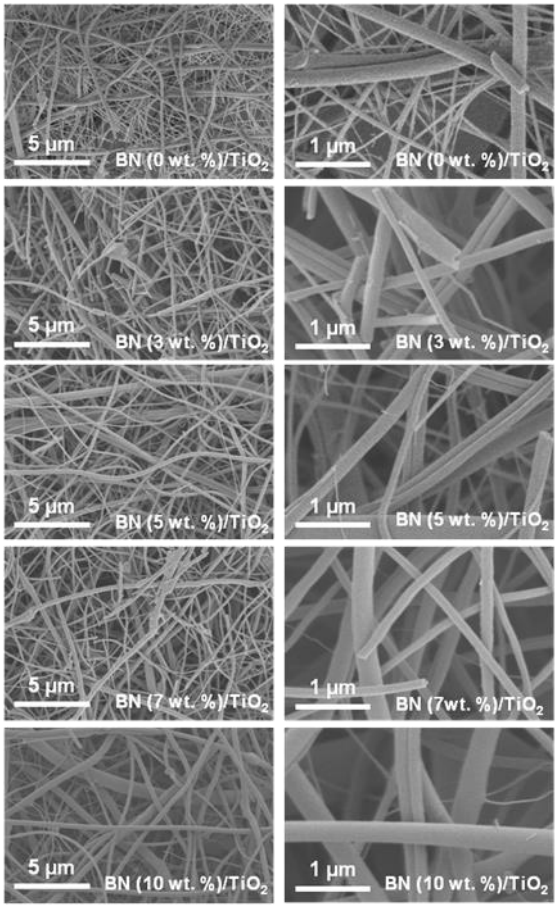

Figure 1. Scanning Electron Microscope images of TiO_2 and BN/TiO_2 annealed composite nanofibers in air for 4h at 500°C

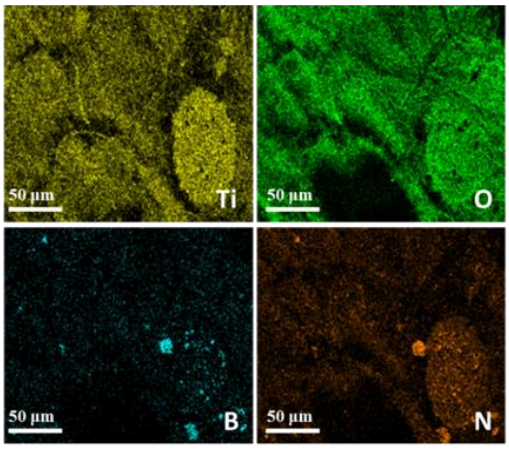

Figure 2. Element mapping images of the BN (5 wt.%)/TiO_2 composite nanofibers

Table 2 presents the specific surface area (BET) of prepared BN/TiO_2 nanocomposites. The specific surface area varies between 19 and 50 m^2g^{-1}. The increasing of the surface area with the increasing of BN sheets amount is clearly seen from Table 2. It is commonly accepted that TiO_2 with a large surface area will have superior photocatalyst activity, because a larger surface area offers more active adsorption sites[36].

Table 2. BET surface area of TiO_2 nanofibers and BN/TiO_2 composite nanofiberss

Samples	Surface area (m^2g^{-1})
TiO_2 NFs	19.66
BN (3wt. %)/TiO_2	31.75
BN (5wt. %)/TiO_2	34.41
BN (7wt. %)/TiO_2	48.31
BN (10wt. %)/TiO_2	49.64

X-ray diffraction (XRD) was employed for analyzing the crystalline phase of all the obtained nanofibers. The sharp peaks in the diffraction pattern of all samples (figure 3-A) can be assigned to the (101), (004), (200), (105), (211) and (204) crystal plane of pure anatase phase of TiO_2 which correspond to 2θ = 25.5°, 38.2°, 48.2°, 54.1°, 55.3° and 62.9°, respectively[6]. It is worth noting that the diffraction peak at 2θ = 26° of hexagonal BN related to the (002) direction is probably overlapped by the diffraction peak of TiO_2 at the same position[37]. The crystallite average sizes of TiO_2 and BN/TiO_2 with different amounts of BN were estimated using the Scherrer equation[38]. The calculated results show that the grain fineness numbers of BN/TiO_2 fibers are increasing as compared to pure TiO_2 fibers. The crystallite sizes for all samples are shown in Table 3.

Table 3. Grain size of TiO_2 NFs and BN/TiO_2 composite nanofibers

	TiO_2	BN (3 wt. %)/TiO_2	BN (5 wt. %)/TiO_2	BN (7 wt. %)/TiO_2	BN (10wt. %)/TiO_2
Grain size (nm)	16.4	24.3	25.2	26.3	28.7

As shown in Figure 3-B, the main TiO_2 peak was shifted from the initial position after BN doping in all samples. We may suppose that BN incorporation increases the lattice strain in the TiO_2 cell and it can shift atoms from the initial position and can reduce the formation of the self-trapped excitons (STE) localized on the TiO_6 octahedral[24]. At the same time, it might cause vacancies formation. These results will be confirmed later by photoluminescence analysis.

Raman spectroscopy is a powerful tool to detect the molecular vibrations in order to identify our materials. As shown in Figure 4, the Raman spectrum of TiO_2, BN (3 wt. %)/TiO_2, BN (5wt. %)/TiO_2, BN (7wt. %)/TiO_2 and BN (10wt. %)/TiO_2 was recorded in the range of 100-1500 cm^{-1}. For all samples, we identify the six Raman active modes corresponding to the anatase phase of TiO_2 at 144 cm^{-1} (E_g), 197 cm^{-1} (E_g), 399 cm^{-1} (B_{1g}), 513 cm^{-1} (A_{1g}), 519 cm^{-1} (B_{1g}) and 639 cm^{-1} (E_g) (figure 4-A)[39]. Besides, the Raman spectra of BN/TiO_2 samples shows the broadened characteristic frequency located at ~ 1365 cm^{-1} referring to the hexagonal BN related to E_{2g} mode (figure 4-B)[40]. In addition, the increased intensity of the peak corresponding to h-BN with the amount of doping is visibly noticed. Thus, Raman spectroscopy confirmed the incorporation of the boron nitride in the TiO_2 nanofibers.

The successful incorporation of boron nitride sheets in the TiO_2 nanofibers was revealed by the typical FTIR spectrum (Figure 5). For pure TiO_2 nanofibers (Figure 5a), the characteristic absorption band at 650–950 cm^{-1} is attributed to Ti–O bond[41]. While for the composite BN/TiO_2 nanofibers with different amounts of BN sheets (Figure 5/b to e), two main absorption peaks of hexagonal BN were observed around 800 and 1370 cm^{-1}, ascribed to the out-of-plane bending of sp^2-bonded B-N-

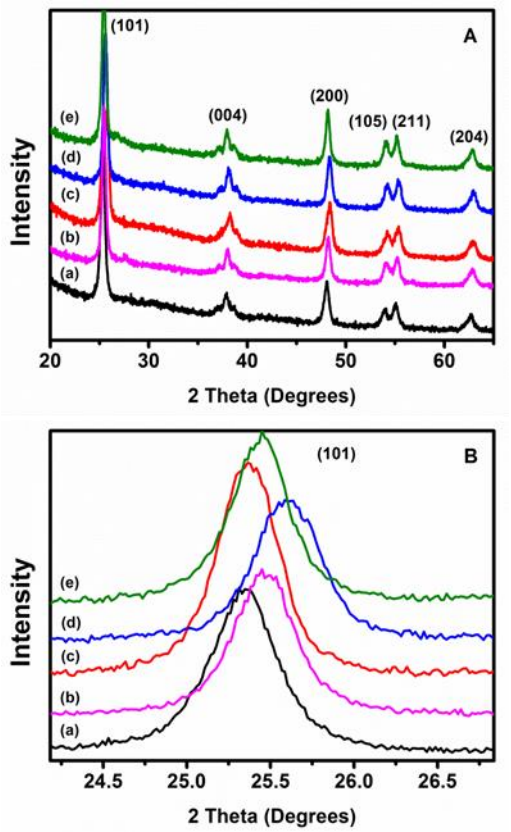

B and the in-plane stretching of sp^2-bonded B-N, respectively[42]. In addition, it can be clearly seen, that the intensity of these 2 peaks related to the bands B-N-B and B-N increases by increasing the BN amounts.

Figure 3. (A-B) XRD patterns of (a) TiO_2, (b) BN (3 wt. %)/TiO_2, (c) BN (5wt. %)/TiO_2, (d) BN (7wt. %)/TiO_2 and (e) BN (10wt. %)/TiO_2 annealed nanofibers in air for 4h at 500°C.

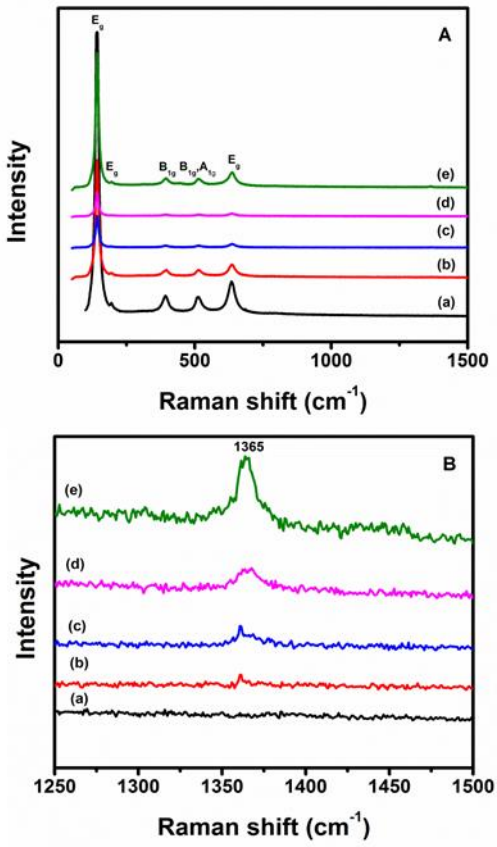

Figure 4. (A-B) Raman shift of (a) TiO_2, (b) BN (3 wt. %)/TiO_2, (c) BN (5wt. %)/TiO_2, (d) BN (7wt. %)/TiO_2 and (e) BN (10wt. %)/TiO_2 annealed nanofibers in air for 4h at 500°C.

Figure 6 shows the UV–VIS absorption spectra of TiO_2 nanofibers and BN/TiO_2 composite nanofiberss with different BN amounts. The energy of the band gap was calculated using the following equation:

$$E_g = hc/\lambda \qquad \text{(Equation 2)}$$

Where h is Planck's constant, c is the speed of light and λ is the cut off wavelength where the absorbance value is minimum. The UV–VIS absorption spectrum of the pure TiO_2 nanofibers, BN (3 wt. %) /TiO_2, BN (5wt. %) /TiO_2, BN (7wt. %) /TiO_2 and BN (10wt. %) /TiO_2 composite nanofibers indicates that it absorbs light at 380, 348, 345, 344 and 342 nm corresponding to a band gap of 3.2, 3.56, 3.59, 3.6 and 3.62 eV, respectively. Compared to the pure TiO_2 nanofibers, the absorption edges of BN/TiO_2 composite nanofibers are blue shifted. These facts suggest that introducing BN sheets may increase the photocatalytic activity of TiO_2 nanofibers under UV light.

PL spectra of TiO_2 nanofibers are shown in Figure 7. The significant increase of the PL intensity was observed for BN (5wt. %)/TiO_2, BN (7wt. %)/TiO_2 and BN (10wt. %)/TiO_2 samples. The PL spectrum of sample BN (3 wt. %)/TiO_2 is approximately equal to the initial TiO_2 PL spectrum. The PL spectra have been deconvoluted to individual peaks with Gaussian fitting using Origin software (Figure 8).

The summary of the PL analysis is shown in the supporting information Table S1. We can distinguish 3 groups of peaks, centred at 415-430 nm, 544-571 nm and 688-731 nm.

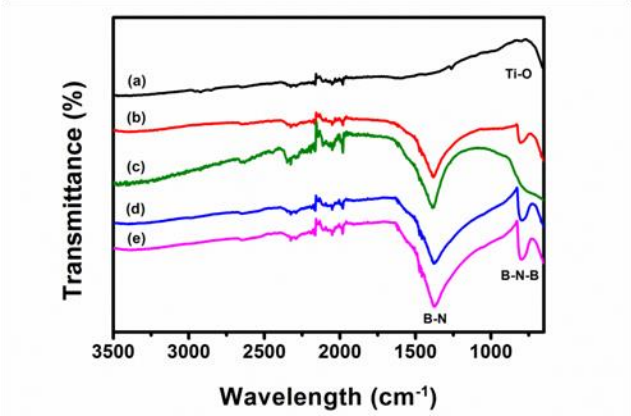

Figure 5. FTIR spectra of (a) TiO_2, (b) BN (3 wt. %)/TiO_2, (c) BN (5wt. %)/TiO_2, (d) BN (7wt. %)/TiO_2 and (e) BN (10wt. %)/TiO_2 annealed nanofibers in air for 4h at 500°C.

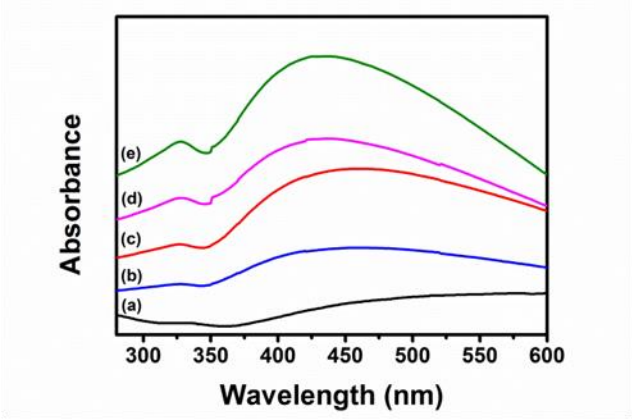

Figure 6. UV-VIS absorption spectra of (a) TiO_2, (b) BN (3 wt. %)/TiO_2, (c) BN (5wt. %)/TiO_2, (d) BN (7wt. %)/TiO_2 and (e) BN (10wt. %)/TiO_2 annealed nanofibers in air for 4h at 500°C.

In our previous works, we have reported on the detailed analysis of the PL spectra of TiO_2 based nanostructures[24,43]. The observed peak at 415-430 nm corresponds to the self-trapped excitons (STE) localized on the TiO_6 octahedral[43,44]. The peaks in the range of 544-571 nm correspond to oxygen vacancies, localized on the surface, and can also be considered as recombination of free electrons with trapped holes. Peaks at 688-731 nm correspond to structural defects (Ti^{3+}, Ti^{3+} interstitials, under coordinated Ti atoms) and can be related to the recombination of free holes with trapped electrons[24,44]. It is worth saying that no peaks related to rutile phase (800-815 nm) were found.

The PL of TiO_2-BN nanostructures have not been reported before. Therefore, the analysis of the PL properties will be based on other photo-induced properties of TiO_2-BN nanostructures. M. Shanmugam *et al.* reported on BN induced passivation of the surface states on TiO_2 when BN-TiO_2 heterojunctions are formed for solar cell applications. It was discussed that BN passivates dangling bonds on the TiO_2 surface and improves the photocatalytic activity of TiO_2 nanostructures[45,46]. The improved photocatalytic activity is based on the charge separation at the TiO_2/BN interface and the flow of holes to the BN upper layer. Thus, it is expected to get lower electron-hole recombination rate in BN doped TiO_2

nanostructures. On the basis of the above mentioned BN-TiO_2 interaction the PL intensity in the BN doped TiO_2 nanostructures should decrease[47,36]. However, in our case, the enhancement of the TiO_2 nanofibers PL was observed when increasing of the doping level of BN.

Figure 7. Photoluminescence of TiO_2 and BN/TiO_2 NFs annealed in air at 500°C.

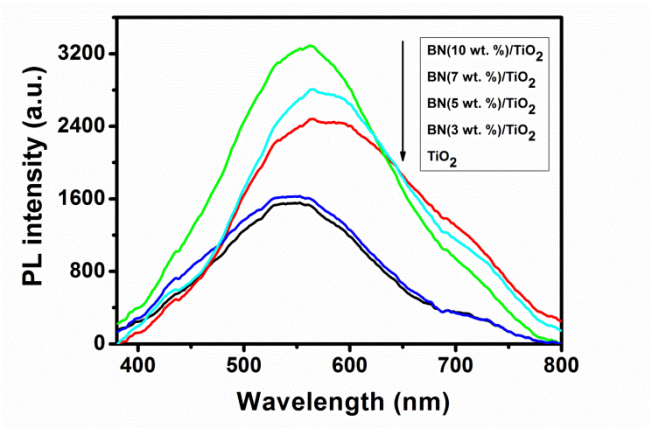

The mechanism of BN doping can be explained from comparison of the deconvoluted TiO_2 PL peaks (Figure 8). Table 4 shows that the normalized integrated STE peak intensity (I1) decreased with the BN doping ratio. From XRD analysis, it was found that additional lattice strain appeared in the TiO_2 lattice after BN doping. The induced strain reduces the formation of the self-trapped excitons (STE) localized on the TiO_6 octahedral and therefore quenches STE emission. The emission related to surface defects (I3) has a tendency to decrease because of the BN passivation of the dangling bonds, related to the unsaturated surface atoms and the photo-generated holes migration to BN[45,47]. We also suppose that BN induced lattice strain in the TiO_2 lattice might cause oxygen vacancies formation. Therefore, the increase of absolute PL value of peaks, related to oxygen vacancies was observed as BN can passivate the surface state of non-radiative recombination and enhance the PL intensity of the whole spectrum. We also assume that due to charge separation on BN-TiO_2 interface, the observed PL emission is due to bulk emission centers rather than surface centers. Thus, the observed results show good correlation between optical and structure properties of BN-TiO_2 nanofibers.

The quantum yield of the samples was calculated as following:

$$QY = N_{em}/N_{abs} \qquad \text{(Equation 3)}$$

Where N_{abs} and N_{em} are numbers of absorbed and emitted photons. Taking into account that all photons are absorbed by TiO_2 at wavelength of 266 nm, no correlation coefficients for N_{abs} were used. The N_{abs} and N_{em} were calculated on the basis of the obtained experimental values, such as laser power, repetition frequency, sensitivity of fiber optic spectrometer per integration time and the measured signal. The obtained values are shown in the Table 5.

Typical QY of TiO_2 nanostructures is in the range of 0.001-0.2, as reported by Li et *al.*[48]. According to the data, obtained in the present work, the QY of TiO_2 nanofibers is one order lower than in other sources. It points to high ratio of charge splitting and non-radiative transitions through surface states[49] what is significantly good for photocatalytic applications.

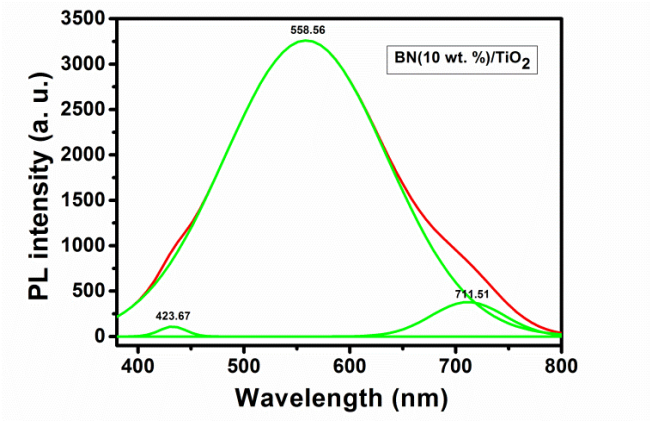

Figure 8. One example of a deconvoluted PL spectrum of BN/TiO_2 NFs annealed in air at 500°C.

Table 4. Normalized integrated intensity of the TiO_2 PL peaks

Doping level	I1	I2	I3
BN (0wt. %)/ TiO_2	0.01481	1	0.05784
BN (3wt. %)/ TiO_2	0.01898	1	0.04002
BN (5wt. %)/ TiO_2	0.00841	1	0.835766
BN (7wt. %)/ TiO_2	0.01279	1	0.15328
BN (10wt. %)/ TiO_2	0.00558	1	0.05248

Table 5. Quantum yield of the pure TiO_2 and BN/TiO_2 composite nanofibers

	TiO_2	BN (3wt. %)/TiO_2	BN (5wt. %)/TiO_2	BN (7wt. %)/TiO_2	BN (10wt. %)/TiO_2
QY($x10^{-6}$)	128	137	210	227	246
Error ($x10^{-5}$)	3.24	3.48	5.34	5.76	6.25

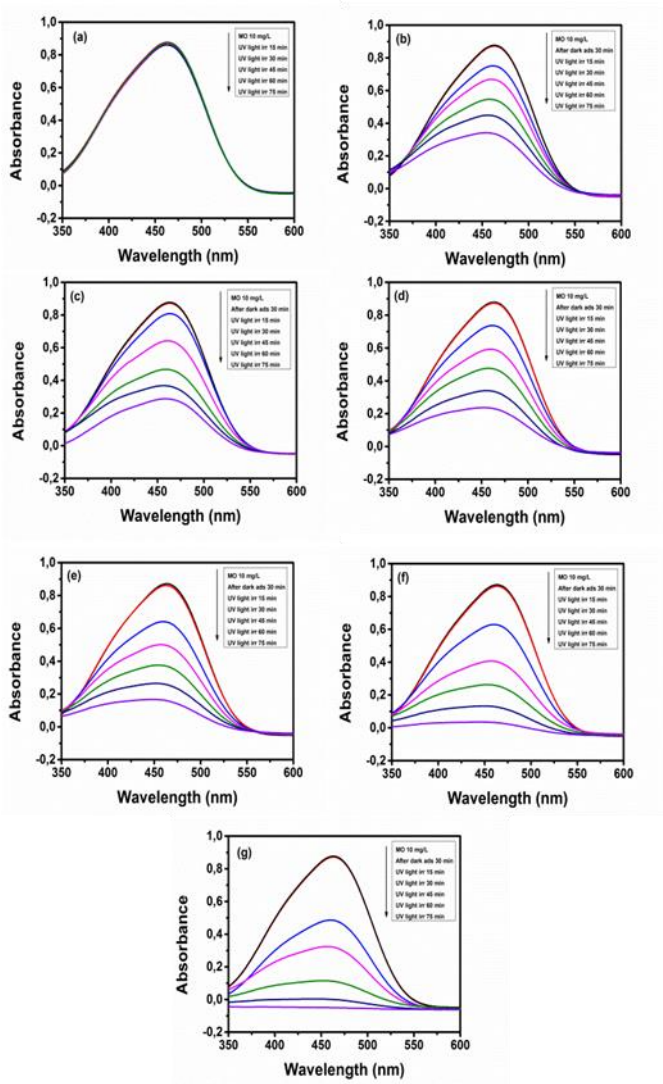

Figure 9. UV-Vis spectra of the photocatalytic degradation of MO under UV light: (a) MO without catalyst, (b) P 25, (c) TiO_2 nanofibers, (d) BN (3wt. %)/TiO_2, (e) BN (5wt. %)/TiO_2, (f) BN (7wt. %)/TiO_2 and (g) BN (10wt. %)/TiO_2 composite nanofibers.

The photocatalytic activities of BN/TiO_2 with different BN amounts were evaluated by degradation of methyl orange (MO) under UV light (wavelength < 400 nm). MO was selected as a model organic pollutant. Figure 9 (a-g) shows the UV-Vis absorbance spectra of MO solution (major absorption band around 462 nm) with different time intervals 0, 15, 30, 45, 60 and 75 min after 30 min storage in dark for excluding the interference of adsorption. For comparison, the photocatalytic activities of TiO_2 nanofibers and commercial TiO_2-P25 were also tested under identical experimental conditions. The results indicate that methyl orange is stable and difficult to be photodegraded in the absence of photocatalyst. After irradiation for 75 min, MO was degraded up to 65% in the presence of TiO_2 nanofibers, compared to 60% degradation by commercial granular TiO_2-P25 (Figure 10). Therefore, in case of pure TiO_2, it is well known that TiO_2 nanofibers have a larger active surface area compared to the commercial TiO_2-P25 nanoparticles which increases its photocatlytic activity[6] . As shown in Figure 10, MO was degraded up to 73%, 80%, 93% and 99% in the presence of BN (3wt. %)/TiO_2, BN (5wt. %)/TiO_2, BN (7wt. %)/TiO_2, BN (10wt. %)/TiO_2, respectively. It is well known that the photocatalytic activity is mainly governed by crystalline phase, specific surface area, light absorption capacity and separation efficiency of electron–hole pairs. Therefore, in BN/TiO_2 samples, owing to the pronounced electrostatic interactions, the surface naturally negative charged of boron nitride sheets could lead to the transfer of h^+ from the activated TiO_2 to the BN sheets when they are connected. Thus, more photo electrons were available compared to pure TiO_2 nanofibers, to take part in the photodegradation process[36,18]. Thus the recombination of e^- and h^+ is inhibited as confirmed previously by photoluminescence. However, considering the specific surface area results of BN/TiO_2 nanofibers presented above, a large increase has been achieved compared to the pure TiO_2 nanofibers. From the XRD analysis, the crystallite average size of TiO_2 is increasing after introducing BN sheets. As confirmed by UV-VIS, compared to the pure TiO_2 nanofibers, the absorption edges of BN/TiO_2 composite nanofibers are blue shifted. From the obtained results, it is evident that BN sheets improve the separation efficiency of e^- and h^+ and therefore enhance the photocatalytic activity of TiO_2 under UV light.

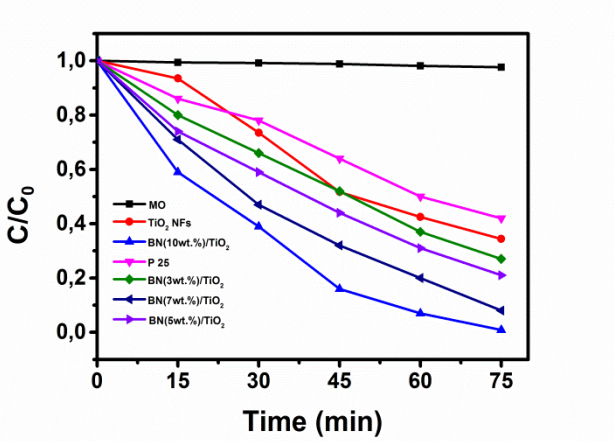

Figure 10. Photodegradation of MO by P25, TiO_2 nanofibers and BN/TiO_2 composite nanofibers

Figure 11 shows the different kinetic linear curves. The photodegradation reactions follow a Langmuir–Hinshelwood first-order kinetics model[1]. The explanation is described as follows:

$$r = dC/dt = kKC/(1+KC) \qquad \text{(Equation 4)}$$

Where r is the degradation rate of methyl orange (MO) (mg $(L\ min)^{-1}$), C is the concentration of the MO solution (mg L^{-1}), t is the irradiation time, k is the reaction rate constant (mg $(L\ min)^{-1}$), and K is the adsorption coefficient of MO (mg L^{-1}). Since the initial concentrations (C_0 = 10 mg L^{-1}) of the MO solutions are very low in the present experiments, the relationship between $\ln(C_0/C)$ and the reaction time t shows that the decomposition of MO with different photocatalysts accords with a pseudo first order kinetic[1]:

$$\ln (C_0/C) = kKt = k_at \qquad \text{(Equation 5)}$$

Where k_a is the apparent first-order rate constant (min^{-1}) and C is the concentration at time t. k_a is obtained from the linear dependence between $\ln (C_0/C)$ and time are reported in Table 6. The increasing order of the rate constants in the samples is: BN (10wt. %)/TiO_2 > BN (7wt. %)/TiO_2 > BN (5wt. %)/TiO_2 > BN (3wt. %)/TiO_2 > TiO_2 NFs > P25. The rate constant exhibits a maximum of 0.0586 min^{-1} for BN (10wt. %)/TiO_2, which is 5 and 3.8 times higher than that of P25 and TiO_2 nanofibers, respectively. In addition, all BN/TiO_2 composite nanofibers show higher

photocatalytic activity than that of P25 and TiO_2 nanofibers under UV light, which is represented by larger value of k_a. Even though, in the case of BN (10wt. %), the curve of [ln (C_0/C) vs time] is not completely linear, it is still considered as approximately following the Langmuir–Hinshelwood model. This behavior is possibly due to the presence of a higher concentration of BN. When the rate of the reaction is increased with additional BN sheets, the adsorption-desorption equilibrium will be slightly disturbed and the Langmuir behavior is therefore shifting from a perfect linear first order. In our case, the disturbance is relatively small and the [ln (C_0/C) vs time] curve is still giving an acceptable value of k_a. From obtained results it is evident that the fact of introducing BN sheets improves separation of photo-induced electron-hole pairs of TiO_2 and significantly increases its photocatalytic activity under UV.

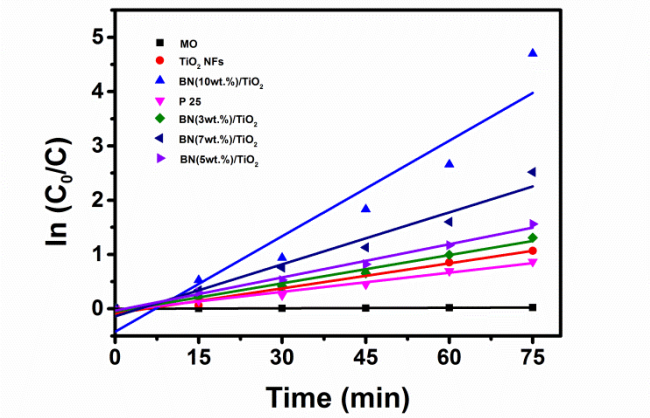

Figure 11. Kinetics of Methyl orange degradation by P25, TiO_2 nanofibers and BN/TiO_2 composite nanofibers

Table 6. Kinetic parameters for photocatalytic activities of the pure TiO_2 nanofibers and BN/TiO_2 composite nanofibers

	k_a (min^{-1})	R^2
MO	0.00031	0.9743
P25	0.0117	0.9791
TiO_2 NFs	0.0153	0.9706
BN (3wt. %)/TiO_2	0.0173	0.9842
BN (5wt. %)/TiO_2	0.0203	0.9900
BN (7wt. %)/TiO_2	0.0319	0.9541
BN (10wt. %)/TiO_2	0.0586	0.8979

Conclusions

In summary, pure TiO_2 nanofibers and BN/TiO_2 composite nanofibers with different BN nanosheets amounts were successfully prepared by electrospinning. All the samples were annealed at 500°C in air for 4 hours. The SEM images showed an increase in the average diameter with the increase of BN amount and confirmed that the one dimensional morphology was maintained. EDX, Raman and FTIR revealed the successful incorporation of the boron nitride in the TiO_2 nanofibers. The specific surface area measurements (BET) confirmed the increasing of the surface area with the increasing of BN sheets amount. A boost of the grain size from 16.4 to 28.7 nm had been recorded for the composite BN (10wt. %)/TiO_2 compared to the pure TiO_2 nanofibers. The increasing of TiO_2 nanofibers band gap energy from 3.2 eV to 3.62 eV due to the presence of BN sheets was confirmed by UV-VIS analysis. XRD and photoluminescence spectra confirmed that BN incorporation increases the lattice strain in the TiO_2 cell and reduce the formation of the self-trapped excitons. Owing to the electrostatic interaction, BN sheets can promote the immigration of h^+ from the bulk of TiO_2 to its surface and consequently improve the photocatalytic activity of TiO_2 under UV light due to efficient charge separation and reduction of charges carriers' recombination. The photocatlytic degradation of methyl orange under UV light was 5 and 3.8 times higher than that of commercial TiO_2-P25 and TiO_2 nanofibers, respectively. In conclusion, the mixing of TiO_2-based photocatalysts with BN sheets is a challenge worth investigating to enhance efficiency in a simple and economically beneficial manner and could be used as catalysts in the degradation of different molecules for photocatalytic application.

Acknowledgements

M. Nasr would like to thank the Lebanese University for the PhD funding. This study was partially supported by the ANR project ANR-14-CE07-0011 "BONALD".

References

1. I. K. Konstantinou and T. A. Albanis, *Applied Catalysis B: Environmental*, 2004, **49**, 1-14.
2. M. J. Nalbandian, M. Zhang, J. Sanchez, S. Kim, Y.-H. Choa, D. M. Cwiertny and N. V. Myung, *Journal of hazardous materials*, 2015, **299**, 141-148.
3. S. Schlicht, L. Assaud, M. Hansen, M. Lickleder, M. Bechelany, M. Perner and J. Bachmann, *Journal of Materials Chemistry A*, 2016, **4**, 6487-6494.
4. D. Spasiano, L. d. P. P. Rodriguez, J. C. Olleros, S. Malato, R. Marotta and R. Andreozzi, *Applied Catalysis B: Environmental*, 2013, **136**, 56-63.
5. C. H. Kim, B.-H. Kim and K. S. Yang, *Carbon*, 2012, **50**, 2472-2481.
6. S. J. Doh, C. Kim, S. G. Lee, S. J. Lee and H. Kim, *Journal of Hazardous Materials*, 2008, **154**, 118-127.
7. V. Štengl, S. Bakardjieva, T. M. Grygar, J. Bludská and M. Kormunda, *Chem. Cent. J*, 2013, **7**, 41.
8. K. R. Reddy, K. Nakata, T. Ochiai, T. Murakami, D. A. Tryk and A. Fujishima, *Journal of nanoscience and nanotechnology*, 2011, **11**, 3692-3695.
9. E. Formo, E. Lee, D. Campbell and Y. Xia, *Nano Letters*, 2008, **8**, 668-672.
10. T. Sreethawong, S. Ngamsinlapasathian and S. Yoshikawa, *Chemical engineering journal*, 2012, **192**, 292-300.

11. X. Xu, G. Yang, J. Liang, S. Ding, C. Tang, H. Yang, W. Yan, G. Yang and D. Yu, *Journal of Materials Chemistry A*, 2014, **2**, 116-122.
12. R. K. Nainani and P. Thakur, *Water Science and Technology*, 2016, **73**, 1927-1936.
13. V. Thangaraj, J. Bussiere, J. M. Janot, M. Bechelany, M. Jaber, S. Subramanian, P. Miele and S. Balme, *European Journal of Inorganic Chemistry*, 2016.
14. M. Öner, A. Çöl, C. Pochat-Bohatier and M. Bechelany, *RSC Advances*, 2016, **6**, 90973-90981.
15. J. Biscarat, M. Bechelany, C. Pochat-Bohatier and P. Miele, *Nanoscale*, 2015, **7**, 613-618.
16. M. Bechelany, A. Brioude, P. Stadelmann, S. Bernard, D. Cornu and P. Miele, *The Journal of Physical Chemistry C*, 2008, **112**, 18325-18330.
17. S. Bernard, V. Salles, J. Li, A. Brioude, M. Bechelany, U. B. Demirci and P. Miele, *Journal of Materials Chemistry*, 2011, **21**, 8694-8699.
18. X. Fu, Y. Hu, Y. Yang, W. Liu and S. Chen, *Journal of hazardous materials*, 2013, **244**, 102-110.
19. Ž. Kesić, I. Lukić, D. Brkić, J. Rogan, M. Zdujić, H. Liu and D. Skala, *Applied Catalysis A: General*, 2012, **427**, 58-65.
20. C. Tang, J. Li, Y. Bando, C. Zhi and D. Golberg, *Chemistry–An Asian Journal*, 2010, **5**, 1220-1224.
21. K. Zhu, N. R. Neale, A. Miedaner and A. J. Frank, *Nano letters*, 2007, **7**, 69-74.
22. S. C. Yang, D. J. Yang, J. Kim, J. M. Hong, H. G. Kim, I. D. Kim and H. Lee, *Advanced Materials*, 2008, **20**, 1059-1064.
23. B. Liu and E. S. Aydil, *Journal of the American Chemical Society*, 2009, **131**, 3985-3990.
24. M. Nasr, A. A. Chaaya, N. Abboud, M. Bechelany, R. Viter, C. Eid, A. Khoury and P. Miele, *Superlattices and Microstructures*, 2015, **77**, 18-24.
25. P. Liang, A. Wei, Y. Zhang, J. Wu, X. Zhang and S. Li, *Micro & Nano Letters*, 2016, **11**, 539-544.
26. K. R. Reddy, B. C. Sin, C. H. Yoo, W. Park, K. S. Ryu, J.-S. Lee, D. Sohn and Y. Lee, *Scripta Materialia*, 2008, **58**, 1010-1013.
27. K. R. Reddy, K. P. Lee, A. I. Gopalan, M. S. Kim, A. M. Showkat and Y. C. Nho, *Journal of Polymer Science Part A: Polymer Chemistry*, 2006, **44**, 3355-3364.
28. X. Wang, C. J. Summers and Z. L. Wang, *Nano Letters*, 2004, **4**, 423-426.
29. G. Tian, Y. Chen, W. Zhou, K. Pan, C. Tian, X.-r. Huang and H. Fu, *CrystEngComm*, 2011, **13**, 2994-3000.
30. K. R. Reddy, V. G. Gomes and M. Hassan, *Materials Research Express*, 2014, **1**, 015012.
31. K. R. Reddy, K. Nakata, T. Ochiai, T. Murakami, D. A. Tryk and A. Fujishima, *Journal of nanoscience and nanotechnology*, 2010, **10**, 7951-7957.
32. C. Eid, E. Assaf, R. Habchi, P. Miele and M. Bechelany, *RSC Advances*, 2015, **5**, 97849-97854.
33. T. P. Dhakal, M. M. Hamasha, A. S. Nandur, D. Vanhart, P. Vasekar, S. Lu, A. Sharma and C. R. Westgate, *Device and Materials Reliability, IEEE Transactions on*, 2012, **12**, 347-356.
34. S. Chuangchote, J. Jitputti, T. Sagawa and S. Yoshikawa, *ACS applied materials & interfaces*, 2009, **1**, 1140-1143.
35. P. Du, L. Song, J. Xiong and H. Cao, *Journal of Materials Science*, 2013, **48**, 8386-8392.
36. V. Štengl, J. Henych and M. Slušná, *Journal of Nanomaterials*, 2016, **2016**, 22.
37. Y. Qiu, J. Yu, J. Yin, C. Tan, X. Zhou, X. Bai and E. Wang, *Nanotechnology*, 2009, **20**, 345603.
38. U. Holzwarth and N. Gibson, *Nature Nanotechnology*, 2011, **6**, 534-534.
39. J. Wang, P. Wang, Y. Cao, J. Chen, W. Li, Y. Shao, Y. Zheng and D. Li, *Applied Catalysis B: Environmental*, 2013, **136**, 94-102.
40. R. V. Gorbachev, I. Riaz, R. R. Nair, R. Jalil, L. Britnell, B. D. Belle, E. W. Hill, K. S. Novoselov, K. Watanabe and T. Taniguchi, *Small*, 2011, **7**, 465-468.
41. L. Thirugnanam, S. Kaveri, M. Dutta, N. V. Jaya and N. Fukata, *Journal of nanoscience and nanotechnology*, 2014, **14**, 3034-3040.
42. Y. Shi, C. Hamsen, X. Jia, K. K. Kim, A. Reina, M. Hofmann, A. L. Hsu, K. Zhang, H. Li and Z.-Y. Juang, *Nano letters*, 2010, **10**, 4134-4139.
43. I. Iatsunskyi, M. Pavlenko, R. Viter, M. Jancelewicz, G. Nowaczyk, I. Baleviciute, K. Załęski, S. Jurga, A. Ramanavicius and V. Smyntyna, *The Journal of Physical Chemistry C*, 2015, **119**, 7164-7171.
44. I. Iatsunskyi, E. Coy, R. Viter, G. Nowaczyk, M. Jancelewicz, I. Baleviciute, K. Załęski and S. Jurga, *The Journal of Physical Chemistry C*, 2015, **119**, 20591-20599.
45. M. Shanmugam, R. Jacobs-Gedrim, C. Durcan and B. Yu, *Nanoscale*, 2013, **5**, 11275-11282.
46. M. Shanmugam, N. Jain, R. Jacobs-Gedrim, Y. Xu and B. Yu, *Applied Physics Letters*, 2013, **103**, 243904.
47. H. Si, G. Lian, J. Wang, L. Li, Q. Wang, D. Cui and C.-P. Wong, *ACS applied materials & interfaces*, 2016.
48. Y. Li, C. Song, Y. Wang, Y. Wei, Y. Wei and Y. Hu, *Luminescence*, 2007, **22**, 540-545.
49. J. Liqiang, Q. Yichun, W. Baiqi, L. Shudan, J. Baojiang, Y. Libin, F. Wei, F. Honggang and S. Jiazhong, *Solar Energy Materials and Solar Cells*, 2006, **90**, 1773-1787.